

AperTO - Archivio Istituzionale Open Access dell'Università di Torino

Pre-flight qualification tests of the Mini-EUSO telescope engineering model

This is a pre print version of the following article:

Original Citation:

Availability:

This version is available <http://hdl.handle.net/2318/1822678> since 2021-12-04T18:41:20Z

Published version:

DOI:10.1007/s10686-021-09805-w

Terms of use:

Open Access

Anyone can freely access the full text of works made available as "Open Access". Works made available under a Creative Commons license can be used according to the terms and conditions of said license. Use of all other works requires consent of the right holder (author or publisher) if not exempted from copyright protection by the applicable law.

(Article begins on next page)

Pre-flight qualification tests of the Mini-EUSO telescope engineering model

February 17, 2021

F. Bisconti^{1,2,*}, H. Miyamoto^{1,2,+}, D. Barghini^{1,2,3}, M. Battisti^{1,2}, A. Belov⁴, M.E. Bertaina^{1,2}, S. Blin-Bondil⁵, G. Cambiè^{6,7}, F. Capel^{8,a}, M. Casolino^{6,7,9}, A. Cellino^{2,3}, L. Conti^{6,10}, G. Contino¹¹, G. Cotto^{1,2}, T. Ebisuzaki⁹, F. Fenu^{1,3}, C. Fornaro¹⁰, D. Gardiol³, P. Klimov⁴, L. Marcelli⁶, M. Mignone², E. Parizot¹², P. Picozza^{6,7}, L.W. Piotrowski^{9,b}, G. Prévôt¹², E. Reali^{6,7}, M. Ricci¹³, K. Shinozaki^{1,14}, F. Simioli¹⁰, G. Suino¹

¹University of Turin, Turin, Italy; ²National Institute for Nuclear Physics Section of Turin, Turin, Italy; ³Italian National Institute for Astrophysics, Astrophysical Observatory of Turin, Turin, Italy ⁴Skobeltsyn Institute of Nuclear Physics, Lomonosov Moscow State University, Moscow, Russia; ⁵Omega, Ecole Polytechnique, CNRS/IN2P3, Palaiseau, France; ⁶National Institute for Nuclear Physics Section of Roma Tor Vergata, Rome, Italy; ⁷University of Roma Tor Vergata, Italy; ⁸KTH Royal Institute of Technology, Stockholm, Sweden; ⁹RIKEN, Wako, Japan; ¹⁰Uninettuno University, Rome, Italy; ¹¹Italian National Institute for Astrophysics - Institute of Space Astrophysics and Cosmic Physics, Palermo, Italy; ¹²Astroparticle and Cosmology lab., Paris Diderot University, French National Centre for Scientific Research, Paris, France; ¹³National Institute for Nuclear Physics Section of Frascati, Rome, Italy; ¹⁴National Centre for Nuclear Research, Lodz, Poland

Abstract

Mini-EUSO is one of the missions of the JEM-EUSO program operating at the International Space Station (ISS). It is a UV-telescope with single-photon counting capability looking at night-time downwards to the Earth through a nadir-facing UV-transparent window. For a part of the pre-flight tests, the Mini-EUSO engineering model has been built, a telescope with 1/9 of the original focal surface and a lens of 2.5 cm diameter. It was used to perform tests before the final design was defined. Tests of the Mini-EUSO engineering model have been made in laboratory and in open-sky conditions. Laboratory tests have been performed at the TurLab facility at the Physics Department of the University of Turin, equipped with a rotating tank. The tank contained different types of materials and light sources. In this way, the configuration for the observation of the Earth from space could be emulated including the Mini-EUSO trigger schemes. Tests related to the possibility of using a JEM-EUSO-type detector for applications such as observation of space debris have also been pursued. Furthermore, observations in open-sky conditions allow the detection and studies of natural light sources such as stars, meteors, planets, and artificial light sources such as airplanes and satellites reflecting the sunlight as well as city lights. Most of listed targets could be detected also with Mini-EUSO. In this paper, the procedures to perform the tests in laboratory and in open-sky conditions are reported, as well as the obtained results. In addition, we discuss the results in view of its contribution to foresee and improve the performance of Mini-EUSO during the operation on board the ISS.

* Corresponding autor: Francesca Bisconti francesca.bisconti@to.infn.it

+ Corresponding autor: Hiroko Miyamoto hiroko.miyamoto@to.infn.it

^a now at: Technical University of Munich, Munich, Germany

^b now at: University of Warsaw, Warsaw, Poland

1 Introduction

Mini-EUSO [1] is the first space-based mission of the JEM-EUSO (Joint Experiment Missions for Extreme Universe Space Observatory) program [2], installed inside the International Space Station (ISS). The JEM-EUSO program is devoted to detect Ultra-High Energy Cosmic Rays (UHECRs) from space, through the fluorescence detection technique and with single-photon counting capability. When charged particles in extensive air showers induced by primary cosmic rays excite nitrogen molecules in the atmosphere, the molecular fluorescence transition leads to the isotropic light emission in the near-UV band (290 – 430 nm), which can be detected with highly sensitive telescopes at nighttime. Moreover, fluorescence detectors observe also the Cherenkov light emitted when charged particles travel with a speed higher than the speed of light in the medium they travel through. The Cherenkov emission occurs along the shower axis and can be observed directly, measuring photons coming from the characteristic Cherenkov cone (by ground-based detectors), or after ground reflection (by high-altitude detectors).

A detector on a satellite would be able to observe the extensive air shower along its development in the atmosphere. Moreover, orbiting around the Earth it would have a full-sky coverage, allowing the direct study of large scale anisotropies and search for their sources, since UHECRs are not significantly deflected by magnetic fields. With a wide field of view, such a detector can increase the probability to detect cosmic rays at the extreme energies with respect to ground-based observatories. In addition, a space-based observatory allows to study a variety of atmospheric phenomena expected to be visible from space, including transient luminous events (sprites, blue jets, elves, etc.), and lightning discharges, as well as meteors and, possibly, samples of strange quark matter (nuclearites) [3]. Ground-based light sources like anthropogenic lights and bioluminescence can also be observed.

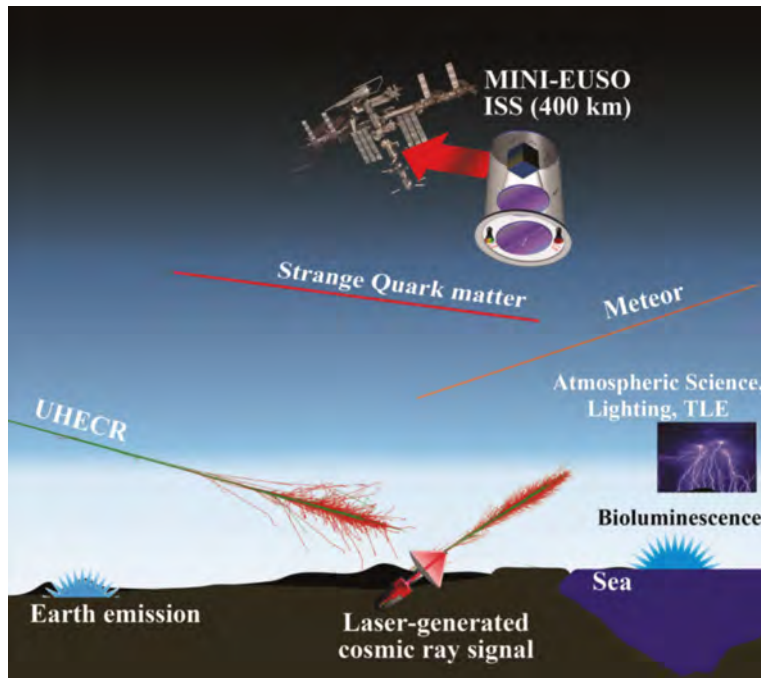


Figure 1: The Mini-EUSO mission with several of its target light sources: emissions from Earth (for example cities), from the sea (bioluminescence), meteors, candidate events to demonstrate the existence of the strange quark matter, atmospheric events, UHECRs, and laser emissions.

To prove the UHECRs detection principle and study the aforementioned phenomena and their possible impact on the detection of UHECRs from space, the Mini-EUSO mission was approved

by the Italian (ASI) and Russian (Roscosmos) space agencies, and has been installed inside the ISS since August 2019, at an altitude of 400 km, behind a UV transparent window in the Russian Zvezda module. It is active since October 2019, performing a few data acquisition sessions per month.

Mini-EUSO and its main science objectives are depicted in Figure 1. Among the other objectives already described for a space-based telescope, Mini-EUSO will provide the mapping of the Earth in the UV band, giving important information on the emissions from the Earth’s surface, which will also represent the background for the detection of other phenomena occurring in the atmosphere. Furthermore, Mini-EUSO can be used to prove the capability of the JEM-EUSO-like telescopes to detect and track space debris. For their high temporal resolutions, such a kind of telescopes are under consideration for the development of a system on a free-flyer satellite for space debris detection, tracking and, in combination with a high-energy laser, possible remediation [4]. To calibrate Mini-EUSO in its final stage onboard the ISS, ground-based lasers shooting in the field of view of the telescope will be used [5][6][7].

A Mini-EUSO engineering model (Mini-EUSO *EM*) was built and tested prior to the finalization of the flight model. The Mini-EUSO *EM* was used in the vibration, electric and electromagnetic interference and compatibility, and thermal-vacuum/environmental tests, while the flight model underwent electric and vibration (at a reduced level) tests [1]. Observations to verify the overall system took place at the Physics Department of the University of Turin and at the Astrophysical Observatory of Turin in Italy, in February and March 2018. At the Physics Department, laboratory tests have been made at the TurLab facility [8] that hosts a rotating tank used to perform analysis with moving light sources. Outdoor observations have been made from the roof of the building, pointing to flashers and lit buildings. Stars, a few meteor candidates, and a large-scale space debris (a derelict rocket body) have been observed from the INAF Astrophysical Observatory, where the sky conditions allowed observation of faint sources, as well as artificial lights from nearby cities. These measurements and related results are presented and discussed in this paper.

2 Detector setup and data acquisitions

2.1 Mini-EUSO design

The Mini-EUSO detector [1] consists of an optical system made of two Fresnel lenses of 25 cm diameter focusing photons on a focal surface with 6×6 Multi-Anode Photo-Multiplier Tubes (MAPMTs) [9], with 8×8 pixels of side 2.88 mm each, for a total of 2304 pixels. The MAPMTs are grouped in 9 Elementary Cells (ECs), made of 2×2 MAPMTs and the frontend electronics. The system of 9 ECs represents the PhotoDetector Module (PDM). The sensitivity band is the near-UV, thanks to a UV bandpass filter 2 mm thick made of BG3 material and with anti-reflective coating. Filters are glued on each single MAPMT, and allow photons with wavelength in the range 290 – 430 nm to reach the sensors. Photos on the top of Figure 2 show the Mini-EUSO detector components, with the external Fresnel lens on the left side and the complete focal surface with 9 ECs, or 36 MAPMTs on the right side. Focal surface and optical system let the detector have a square field of view of $44^\circ \times 44^\circ$, allowing for observations of the Earth with a spatial resolution of ~ 6 km projected on ground. Each EC consists of 4 MAPMTs, each with independent EC-Anode board and a single high voltage power supply with EC-Dynode distribution board, common for 4 MAPMTs. Signals are pre-amplified and digitalized by one 64-channel ASIC chip (SPACIROC3) [10] per MAPMT. Small gaps between MAPMTs of the same EC are required by mechanical fixations, as well as electric insulation in case of a MAPMT failure, while gaps between ECs are mostly due to electric insulation and mechanical fixation.

Data are sampled in Gate Time Units (GTUs), $2.5 \mu\text{s}$ long, and saved with three time resolutions, to cover the different timescales typical of the various phenomena Mini-EUSO aims to observe. Namely, D1 GTU refers to the aforementioned GTU ($2.5 \mu\text{s}$), D2 GTU refers to $128 \times 2.5 \mu\text{s}$ ($320 \mu\text{s}$), and D3 GTU corresponds to $128 \times 128 \times 2.5 \mu\text{s}$ (40.96 ms). For each pixel, the number of

counts collected in single D2 and D3 GTUs is the sum of counts collected over the corresponding number of D1 GTUs (128 for D2 GTUs and 128×128 for D3 GTUs). The D1 and D2 timescale events have dedicated trigger logics devoted to their detection, L1 and L2 trigger respectively [11][12], while a continuous acquisition of the signal integrated over D3 GTUs is performed. The L1 trigger analyzes data with a time resolution of 1 D1 GTU and looks for signal excess on a timescale of $20 \mu\text{s}$ (8 D1 GTUs). This is the typical timescale of cosmic-ray-like events, also well suitable for the detection of elves and flashers with timescales of $\sim 0.01 - 1 \text{ ms}$ [1]. Data integrated over 128 D1 GTUs are used to determine the background level and, at the same time, they are passed to the L2 trigger logic, well-suited to capturing atmospheric events such as lightning with timescales of $\sim 1 - 100 \text{ ms}$ [1]. Packets of 128 D1 GTUs are stored as D2 data in case of L2 triggers. A continuous acquisition of 128×128 D1 GTUs are also stored as D3 data. During the further accumulation of 128 D3 GTUs (5.24 s in total) up to four events detected with the L1 and L2 triggers are stored and transferred to the CPU together with the D3 data, for formatting and storage on the disk. In this way, a continuous readout is achieved with a resolution of 40.96 ms whilst also recording interesting events at shorter timescales. Data frames integrated over D3 GTUs are used to search for meteors, space debris and strange quark matter, as well as for the mapping of the Earth in the near-UV.

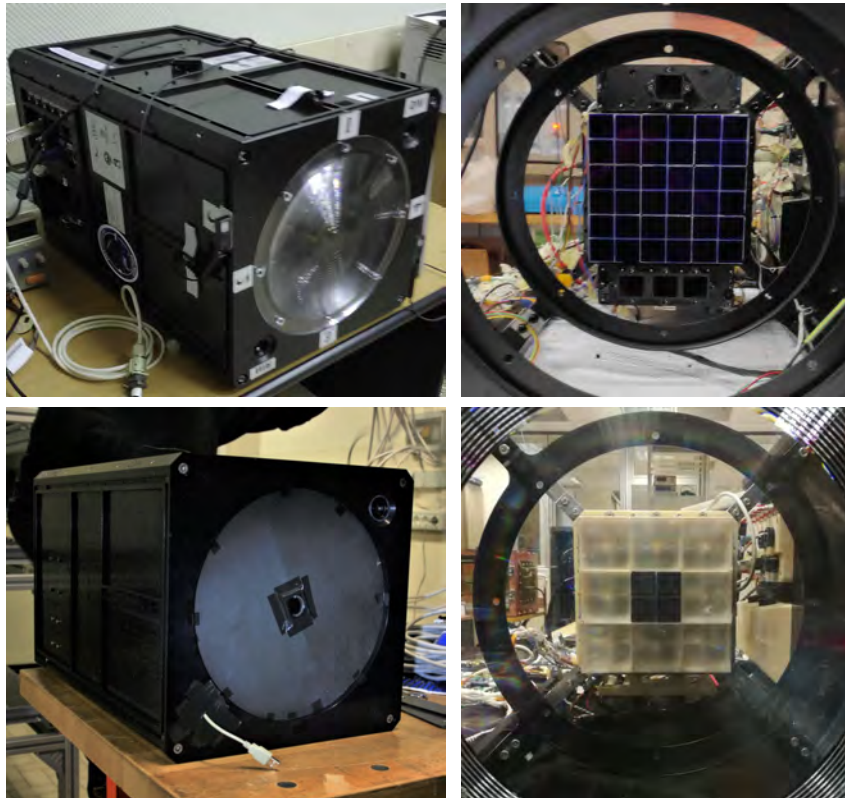


Figure 2: Mini-EUSO exterior view, with the Fresnel lens of 25 cm diameter (top-left); the internal focal surface made of 6×6 MAPMTs (top-right). The Mini-EUSO *EM* exterior view, with the lens of 2.5 cm diameter (bottom-left); the internal focal surface made of 2×2 MAPMTs (bottom-right). Photos of Mini-EUSO taken from [1].

2.2 The Mini-EUSO *EM* design

The Mini-EUSO *EM* is a detector similar to the Mini-EUSO flight model but with a plano-convex lens of 2.5 cm diameter and 30 cm focal length as optical system, and a focal surface corresponding to the central EC of the Mini-EUSO focal surface. The decision of using a different lens system with respect to Mini-EUSO was made to avoid the risk of damaging the original Fresnel lenses. Since the main goal of the data acquisitions was to test the performance of the electronics, the loss in terms of light collection caused negligible consequence. Also the Mini-EUSO *EM* has a square field of view but it is $\sim 10^\circ \times 10^\circ$, due to the reduced focal surface and the different optics. In the pictures shown on the bottom of Figure 2 the exterior of the Mini-EUSO *EM* is visible on the left side, including the lens at the center of the front side, while its focal surface is shown on the right side, composed only by the central EC.

The read-out system and the trigger logics used for the Mini-EUSO *EM* are the same as those for the flight model. In the same way, data are sampled on three time scales with resolution 2.5 μ s, 320 μ s and 40.96 ms.

2.3 Flight model vs. engineering model of Mini-EUSO

In the previous subsections, technical information on the Mini-EUSO *EM* and Mini-EUSO have been reported. Here, a comparison of their performance is provided, based on the difference of the two setups. Table 1 summarizes the comparison of key specifications of the engineering and flight models.

	Mini-EUSO <i>EM</i>	Mini-EUSO
Focal Surface	2 \times 2 MAPMTs 16 \times 16 = 256 pixels	6 \times 6 MAPMTs 48 \times 48 = 2304 pixels
Optical system	1 plano-convex lens	2 Fresnel lenses
Diameter lens(-es)	2.5 cm	25 cm
Focal length	30 cm	20.5 cm
Focal ratio	$f/12$	$f/1.2$
Field of view	square	square
Total	$\sim 10^\circ \times 10^\circ$	$\sim 44^\circ \times 44^\circ$
Per pixel (no gaps)	$\sim 0.6^\circ \times 0.6^\circ$	$\sim 0.8^\circ \times 0.8^\circ$

Table 1: Comparison of the key specifications of Mini-EUSO *EM* and Mini-EUSO.

As the lens size of the Mini-EUSO *EM* is 1/10 of that of Mini-EUSO, the first is 100 times less sensitive than the latter. The table contains also the focal ratio, defined as the ratio between the focal length and the diameter of the aperture, parameter usually adopted for optical systems to define their sensitivity.

The field of view of the Mini-EUSO *EM* ($10^\circ \times 10^\circ$) was estimated from the position of stars detected during outdoor measurements. Instead, the field of view of Mini-EUSO ($44^\circ \times 44^\circ$) was formerly estimated with simulations during the designing phase, then confirmed with measurements from space using cities as reference. Considering the gaps between the MAPMTs, the field of view of one pixel results to be $\sim 0.8^\circ \times 0.8^\circ$ for Mini-EUSO and $\sim 0.6^\circ \times 0.6^\circ$ for the Mini-EUSO *EM*. As the single-pixel field of view of Mini-EUSO is approximately twice that of the Mini-EUSO *EM* ($0.8^2/0.6^2 \simeq 1.8$), the amount of background light collected by one pixel of the first detector is about twice the background collected by the latter. This leads to signal-to-background ratio for the Mini-EUSO *EM* about twice that of Mini-EUSO, due to the field of view difference only and considering the signal from a point-like source. Therefore, considering both the optics and field of view factors, the signal-to-background ratio of the Mini-EUSO *EM* is $\sim \sqrt{2/100} \simeq 1/7$ that of Mini-EUSO. Such estimation was made taking into account the same background intensity and the same light source apparent intensity.

3 Tests at TurLab

3.1 TurLab and the EUSO@TurLab project

TurLab is a laboratory designed for geo-fluid-dynamics studies that hosts a tank where planetary atmospheric phenomena and fluid instabilities can be reproduced by means of inks or suspended particles in the water. The tank is 5 m diameter and has the capability of rotating at speeds ranging from 3 s to 20 min per rotation. Moreover, as it is located in a very dark environment, the intensity of background light can be adjusted in a controlled condition.



Figure 3: The TurLab tank setup with the Mini-EUSO *EM* installed on the ceiling and enlarged inside the red frame (left). The diffused airglow in the atmosphere was represented with two strips of cold-white LEDs reflected by the ceiling above the tank (right).



Figure 4: Light sources and materials to reproduce phenomena that Mini-EUSO can observe are visible. Reflections of materials that are often present in space debris (SD) have also been tested.

A series of measurement campaigns devoted to test several prototypes and pathfinders of the JEM-EUSO program have been performed at TurLab [13][14]. These telescopes are designed to observe the Earth's atmosphere from the stratosphere or from space. By hanging the telescope on the ceiling above the rotating tank (see Figure 3), it is possible to mimic a detector in orbit observing the Earth. In this environment, it is possible to test the performance of the electronics and the L1 trigger for cosmic rays, considering different background conditions, as well as the response to atmospheric phenomena such as meteors and lightning reproduced in the laboratory.

3.2 The Mini-EUSO *EM* at TurLab

In February and March 2018, the Mini-EUSO *EM* was tested at TurLab. After preliminary operation tests at its arrival, it was hung on the ceiling above the TurLab tank to be tested for its general performance as well as for the data acquisition and control software [11] and the trigger system [12].

The setup for the TurLab measurements is shown in Figure 3. In the central panel the TurLab tank is shown, and on top of it, the detector to be tested is installed on the ceiling as shown in the area surrounded by a red frame in the left panel. The pictures in Figure 4 show the light sources and materials reproducing the various phenomena that Mini-EUSO is able to observe from space. In Table 2 materials and phenomena reproduced in the laboratory are listed with the corresponding mean of emulation. All materials were illuminated by diffused light, emitted by two strips of cold-white LEDs and reflected by the ceiling above the tank (Figure 3 on the right), to reproduce the diffused airglow in the atmosphere at the level of expected photon counts that Mini-EUSO would have observed (~ 1 count/pixel/D1 GTU).

Materials and phenomena	Means of emulation
rocks	bricks
deserts	sand
glacier ice	smashed glass
clouds	clusters of particles floating in the water
forests	moss
lightning	smashed glass
city lights	LED light through the holes on the map of Turin city
meteors	Lissajous figures generated by an analogue oscilloscope
cosmic rays	Arduino-driven LED strip
space debris	aluminum foil, copper foil, mirror, white paper, Kevlar [®] , electronics board

Table 2: List of materials or phenomena reproduced in TurLab with the corresponding means of emulation.

By rotating the tank, it was possible to reproduce the Mini-EUSO observation of the Earth on the ISS orbit. In Figure 5 the light curve relative to the measurements by Mini-EUSO *EM* during one TurLab tank rotation (~ 2 min long) is visible, with time resolution of 1 D3 GTU. In D3 data light from all the materials in the field of view is recorded as a continuous “movie”, so the light curve represents the number of counts collected in each D3 GTU by the detector while the TurLab tank was rotating below it.

3.2.1 Tests on the L1 trigger

The L1 trigger allows the detection of cosmic-ray-like events, looking for signal excess on 8 consecutive D1 GTUs ($20 \mu\text{s}$). For each pixel, the signal integrated over 128 D1 GTUs ($320 \mu\text{s}$) is used to determine the average background level per D1 GTU \bar{n} , and therefore the average background counts integrated over 8 consecutive D1 GTUs is $\bar{n}_8 = \bar{n} \times 8$. The trigger threshold is calculated as $T_{trig} = \bar{n}_8 + m \cdot \sqrt{\bar{n}_8}$, where the term $\sqrt{\bar{n}_8}$ is the standard deviation of the Poisson distribution of the counts integrated over 8 D1 GTUs, and m is an integer number that can be used as parameter to define the trigger performance, initially set to $m = 8$. In order to have a trigger, an event has to generate a number of counts integrated over 8 consecutive D1 GTUs greater or equal to the rounded up threshold. In such a case, a packet of 128 D1 GTUs around the triggered event is saved: as 64 D1 GTUs are saved before and after the trigger, the D1 GTU at which the trigger condition is satisfied is the 64th of the packet. In very low background condition, i.e. ≤ 0.3 counts/pixel/D1 GTU, the threshold is set to 15 counts, which is the threshold corresponding to 0.3 counts/pixel/D1 GTU.

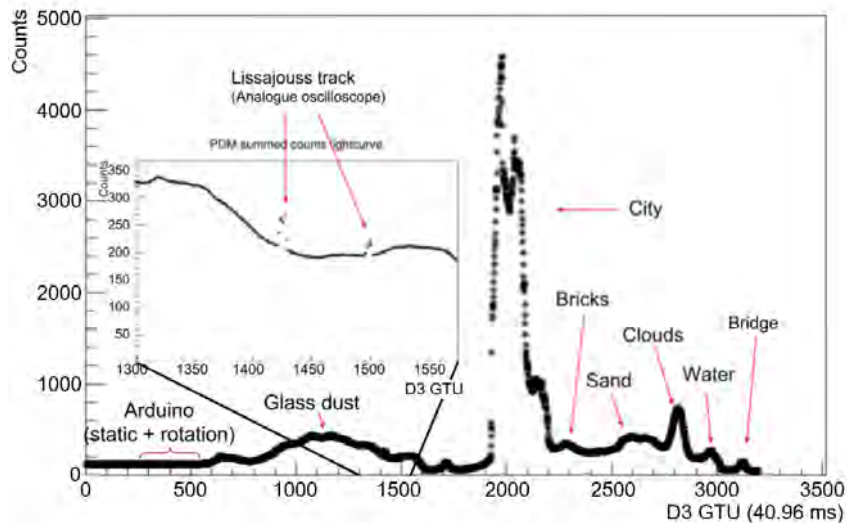


Figure 5: Light curve of D3 data for a whole tank rotation with a speed of ~ 2 min/rotation. All the materials in the field of view are recorded as a continuous “movie”. The “Bridge” signature is due to light reflected by a mechanical structure of the tank, partially visible although it was covered by black fabrics to hide it, as not of interest in the context of the measurements.

Some pixels with very low background have been used to test the trigger functionality, for which the expected threshold was of 15 counts. In Figure 6, the light curve of one pixel which has very low background counts is shown. Summing up the counts of the last 8 D1 GTUs, at the D1 GTU 63 (the 64th of the packet starting counting from D1 GTU 0) the threshold value is reached (with 16 counts with respect to a threshold of 15 counts), and therefore this event was recorded. In Figure 7, the light curve of a pixel with background ~ 0.6 counts/pixel/D1 GTU is shown. In this case, the threshold is higher than the default minimum one, and results to be 23 counts. At D1 GTU 63, the sum of the counts over the last 8 D1 GTUs (30 counts) is above threshold, and therefore the event was triggered.

Tests performed with the Mini-EUSO *EM* at TurLab showed that the average trigger rate was around 10 Hz, much higher than the required limit of 0.75 Hz. For this reason, subsequent tests using a system similar to the Mini-EUSO *EM* have been performed. These tests indicated that to keep the trigger rate below 0.75 Hz at all background levels (from ≤ 0.3 counts/pixel/D1 GTU to city lights), the m parameter in the formula to calculate the threshold had to be fixed to $m = 16$.

3.2.2 Tests on the L2 trigger and D3 continuous data acquisition

Unlike the L1 trigger, which still had to be improved and debugged in its logic, the L2 trigger was found to work as expected. Bright events lasting relatively long such as Lissajous figures produced by an analogue oscilloscope, which can give similar time profiles to those of transient luminous events, were detected using the L2 trigger. It also triggered on the mimicked city light, as the light increased rapidly when it entered the field of view of the detector from inside the tank, but any other material or light source such as glass dust or the Arduino-driven LED strip did not generate any trigger, i.e. no fake triggers occurred during this test.

Also, as shown in Figure 5 for the D3 data, a continuous data acquisition was stored during the measurements, and each illuminated material and light source can be clearly recognized in the light curve. In Figure 8 samples of observations made in D3 scale are shown. The first panel shows the signal from a meteor reproduced by the Lissajous figures of an analogue oscilloscope, after the integration over 20 D3 data frames in order to have the whole track in one frame. The other two panels show smashed glass reproducing glacier ice, and sand reproducing desert.

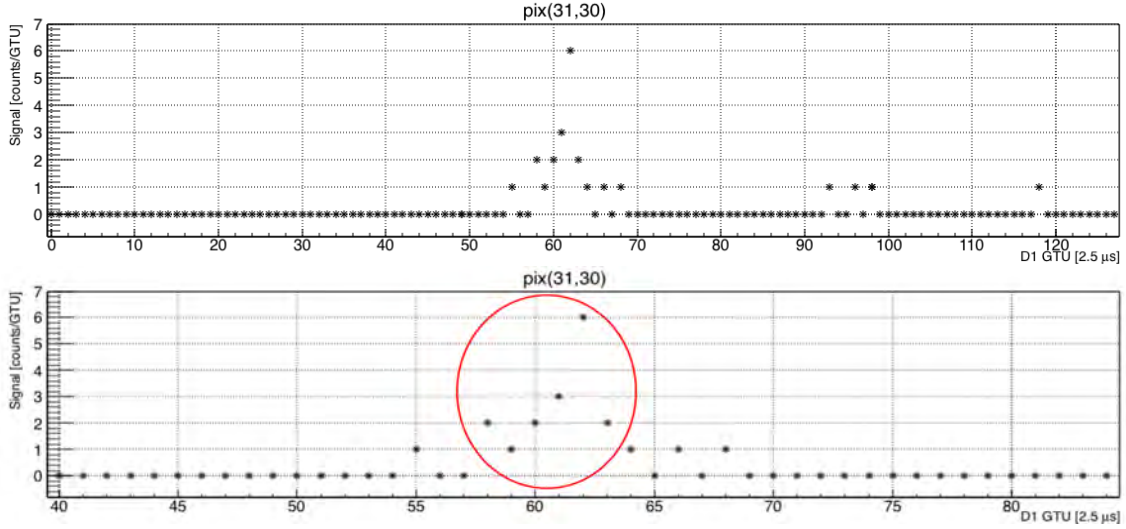


Figure 6: Light curve of D1 data related to one pixel with very low background ~ 0.3 counts/pixel/D1 GTU. In the top panel, the light curve of 128 D1 GTUs containing the triggered event is shown, and in the bottom panel a zoom-in on the event is presented. The counts integrated over 8 consecutive D1 GTUs reach the threshold of 15 counts (16 counts in the red circled area), which is the minimum threshold in very low background condition, and therefore this event was recorded.

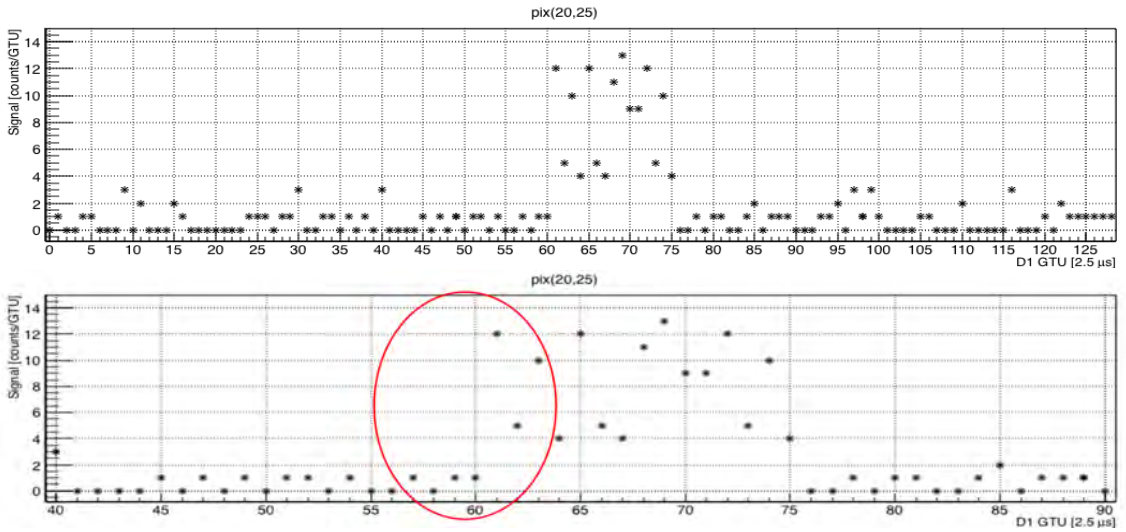


Figure 7: Light curve of D1 data related to one pixel with background ~ 0.6 counts/pixel/D1 GTU. In the top panel, the light curve of 128 D1 GTUs containing the triggered event is shown, and in the bottom panel a zoom-in on the event is presented. The counts integrated over 8 consecutive D1 GTUs reach the threshold of 23 counts (30 counts in the red circled area), and therefore this event was recorded.

3.2.3 Measurements for space debris studies

Space debris do not emit light themselves but can be detected if illuminated by sunlight, at twilight. A special setup to reproduce the space debris detection with the Mini-EUSO *EM* was also designed at TurLab. Measurements of the reflectivity of materials which usually compose space debris

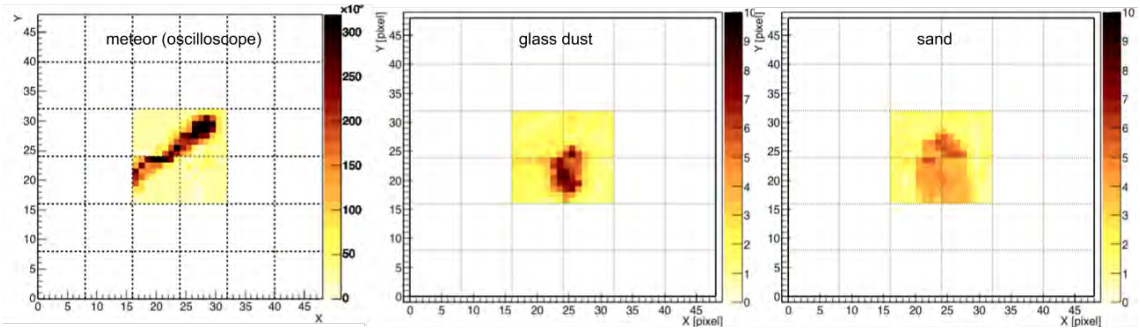


Figure 8: Examples of D3 data frames of Lissajous figures of an analogue oscilloscope, smashed glass, and sand. In the case of the Lissajous figures, it is an integrated image on 20 D3 GTUs to make the moving track visible in one data frame, while the other two refer to a single D3 GTU frame.

(shown in the bottom-left of Figure 4) were performed [16]. For these tests, the Mini-EUSO *EM* was hung on the ceiling above the tank pointing downward. Different materials such as polished and unpolished aluminum foil, canned aluminum, balled aluminum foil, copper foil, mirror, white paper, a sample of Kevlar[®], electronics board (all materials that often space debris are composed of), were placed on the bottom of the tank, and illuminated by diffused light with different intensities. In this way, it was possible to measure the relative reflectance of the materials as seen by the detector. As a preliminary estimation, assuming that the reflectivity of polished aluminum is about 0.92, we observed the reflectance of the different materials varying from 0.17 (electronics board) to 0.92 (fixed reference value for the polished aluminum foil).

Simulation studies applying a dedicated trigger algorithm indicated the capability of Mini-EUSO to observe and track space debris. By using ESAF (EUSO Simulation and analysis Framework) [17] an estimation of the minimum sizes and maximum distances of detectable space debris was made [16]. Furthermore, it was possible to study the number of expected space debris detections using an ESA software called MASTER (Meteoroid and Space debris Terrestrial Environment Reference) [18], which provides the density of space debris with parameters such as altitude and inclination. The potential of a Mini-EUSO-like detector was evaluated with a rate of hundreds of space debris per year [16]. An important contribution was provided by the detection of a real space debris with the Mini-EUSO *EM* during a data acquisition session at the Astrophysical Observatory of Turin, discussed in Section 4.3.2. Size and distance of this derelict rocket have been rescaled in order to reproduce the detection of space debris with Mini-EUSO on-board the ISS. These studies are of fundamental importance to verify the working principle of a space-based system under development for the detection and remediation of space debris [4].

4 Measurements in open sky conditions

4.1 Mini-EUSO*EM* at the Astrophysical Observatory of Turin

The Astrophysical Observatory, located at Pino Torinese on a hill nearby Turin, offers good conditions for the observation of the sky, as city lights are relatively far away and at lower altitude with respect to the observatory site. Moreover, it hosts one all-sky camera of the Italian network for systematic surveillance of meteors and atmosphere, PRISMA [19].

The PRISMA network is devoted to the observation of fireballs in the sky, with the goal of recovering on ground the meteorites surviving the ablation in the atmosphere. The PRISMA network recovered its first meteorite on 4 January 2020, thanks to precise computation of the area where to search for fragments (strewn-field) generated by a bolide seen by eight cameras of the

**2018/03/13
03:13:59UTC**

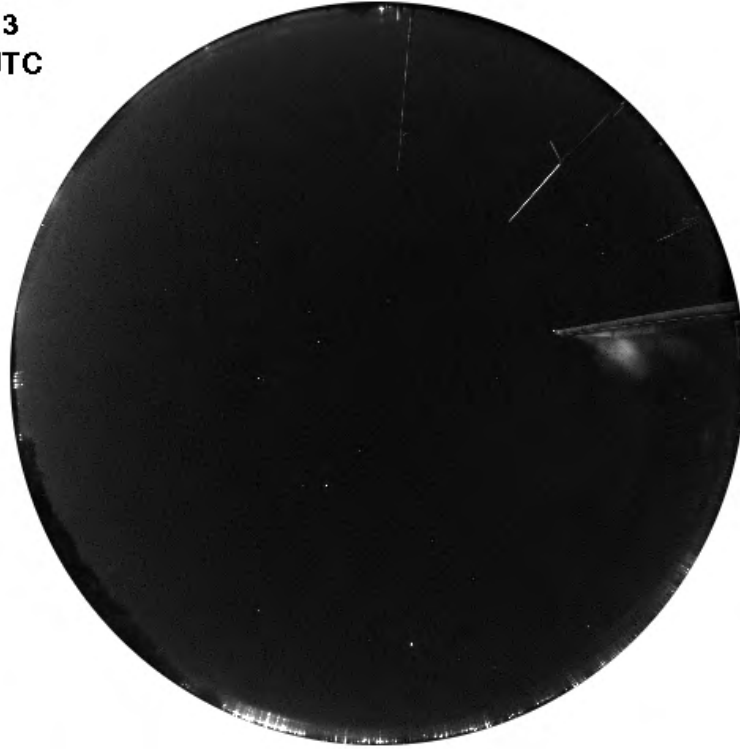


Figure 9: An image taken by the PRISMA camera during the Mini-EUSO *EM* data acquisition campaign of 13 March 2018. The image is integrated over 5 s for the observation of stars. On the edge, bright spots correspond to the nearby urban areas. A flag and antennas present at the PRISMA camera site are visible on the top-right in the field of view.

network on 1 January 2020 at 18:26:53 UTC. This is the first meteorite recovered thanks to a fireball network in Italy, and one of twenty in the world so far [20].

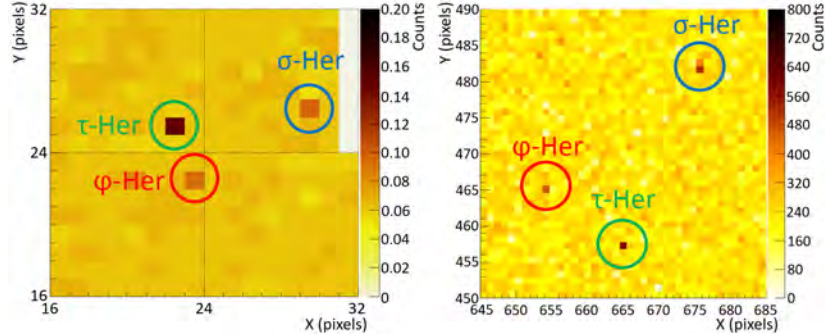
The PRISMA cameras observe the sky with a large wavelength bandwidth peaked in the visual band and with an angular resolution of $\sim 0.2^\circ \times 0.2^\circ$ /pixel [21]. They operate with a high frequency of 30 frames/s (with 1/30 s exposure time) to follow the development of fireballs properly. At this exposure time, stars are not visible. Therefore, additional ancillary images integrated over 5 s are saved every 10 minutes, in order to use star images to derive both astrometric and photometric calibration of the instrument [22]. In Figure 9 one of such all-sky images for the observation of stars is shown. On the edge of the image, bright spots correspond to the nearby urban areas. Slow events such as planes or satellites are not recorded, as they are rejected by the trigger algorithm specifically designed for meteor detection.

A comparison of the stars observations with the PRISMA camera and the Mini-EUSO *EM* was made to understand the relative performance of the two detectors, also in view of possible future simultaneous observations of meteors with PRISMA cameras from the ground and Mini-EUSO from the ISS. A comparison of the rising signal at dawn time was also performed. In addition, faint meteors and the rocket body of a telecommunication satellite were observed by the Mini-EUSO *EM*, but not by the PRISMA camera, because they were rejected by the trigger algorithm.

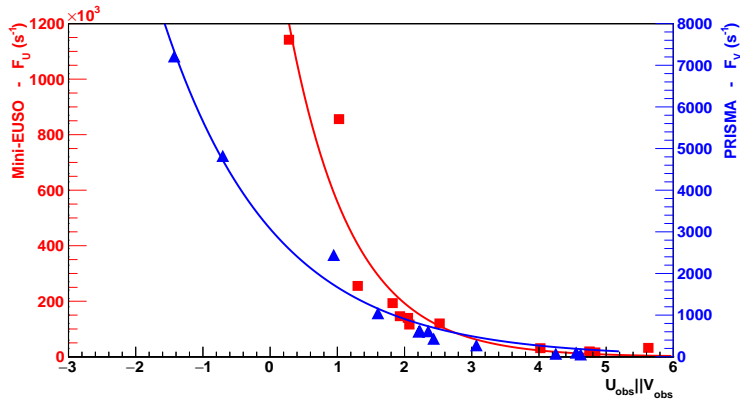
4.2 Natural sources

4.2.1 Stars and planet

Several stars and the planet Jupiter have been identified in the data taken with the Mini-EUSO *EM* from the Astrophysical Observatory by pointing at different zenith angles during the nights of data acquisition. By comparing the cataloged positions of stars with the observations, it was possible to estimate the field of view of the instrument. In particular, three stars of the Hercules



(a) Three stars of the Hercules constellation seen by Mini-EUSO *EM* (left) and the PRISMA camera (right)



(b) Count rates from stars and Jupiter

Figure 10: (a) Stars of the Hercules constellation in a Mini-EUSO *EM* data frame integrated over 40.96 ms (left) and in an image of the PRISMA camera integrated over 5 s (right). The images have to be mirrored and rotated by a few degrees to have the same orientation. (b) Count rates from stars and Jupiter for the Mini-EUSO *EM* (red squares and left y-axis) and for the PRISMA camera (blue triangles and right y-axis), with respect to the U (for the Mini-EUSO *EM*) and V (for PRISMA) apparent magnitudes.

constellation that were captured in the same data frame were used to estimate the total field of view of $\sim 10^\circ \times 10^\circ$, or $\sim 0.6^\circ \times 0.6^\circ$ /pixel excluding the gaps between MAPMTs. In Figure 10 three stars of the Hercules constellation are shown in the (a) panel: the image on the left is a data frame of the Mini-EUSO *EM* integrated over 40.96 ms and the one on the right is a data frame of the PRISMA camera integrated over 5 s. The images have to be mirrored and rotated by a few degrees to have the same orientation. The (b) panel shows the count rates from the observed stars and Jupiter for the Mini-EUSO *EM* (red y-axis on the left) and for the PRISMA camera (blue y-axis on the right), with respect to their U (for the Mini-EUSO *EM*) and the V (for PRISMA) apparent magnitudes, respectively. The apparent magnitudes have been corrected for

the atmospheric attenuation, depending on the altitude of the stars above the horizon. Data points have been fitted with an exponential function with base-10, as the magnitudes are proportional to the base-10 logarithm of the flux. In general, the Mini-EUSO *EM* was sensitive to apparent magnitudes up to about +4 from astronomical catalog, or even greater once they are corrected for the atmospheric attenuation. The simultaneous observations of stars, i.e. with the same atmospheric condition, allows to compare the observations made with the two detectors. This would be useful in the case of simultaneous observation of meteors by Mini-EUSO from space and by the PRISMA cameras on ground or other meteor observatories that might operate in a similar manner. Indeed, usually meteors are observed in the visual band, and the observation in the UV band could give more information about the development of meteors in the atmosphere. Moreover, observations from very different viewing angles during their development could improve the understanding of these phenomena. More details on the observation of meteors with Mini-EUSO are available in [23].

4.2.2 Meteors

Four meteor candidate events have been detected while the Mini-EUSO *EM* was pointing in the zenith direction at the Astrophysical Observatory. From the comparison with the brightness of stars, they had apparent magnitudes of about +4. There is no counterpart of these events in the data of the PRISMA camera, as it is not sensitive to such faint meteors. Indeed, its limit for the apparent magnitude is about -1, or even about 0 with the best sky conditions. However, as the meteor candidates developed at zenith, it was possible to estimate the horizontal component of their speed, supposing that the development of meteors starts at ~ 100 km altitude. The horizontal component of the speed was estimated as tens of kilometers per second, consistent with the actual meteors speed.

In Figure 11 one of the candidate meteors is visible, moving through four consecutive D3 data frames in the top MAPMTs along 8 pixels, from right to left. The duration of this event was ~ 160 ms (~ 20 ms/pixel) and the estimated horizontal speed was ~ 50 km/s.

4.2.3 Night sky brightness

The observation of the night sky from the Astrophysical Observatory lasted until the dawn. The increase of the luminosity is clearly detected by both the Mini-EUSO *EM*, while it was pointing to zenith, and the PRISMA camera. In Figure 12 the night sky count rate of the four MAPMTs of the Mini-EUSO *EM* and of the PRISMA camera over the time are shown. The latter is normalized to the mean value of the three MAPMTs with lower counts. At the dawn, the counts increased first in UV and then in visual band. This can be explained considering that UV photons in the atmosphere are more scattered than visible ones. Therefore, with the Sun approaching the horizon before sunrise, stronger flux of scattered light would be observed at zenith in UV rather than in the visual band. Peaks in the green line between 01:30 and 02:00 UTC correspond to a star crossing eight pixels of a MAPMT; the valleys correspond to the edges between adjacent pixels, in which the sensors are less sensitive.

4.3 Artificial sources

4.3.1 Lit signs, flashes and city light

Artificial lights from the nearby urban area could be also used to test the detector. From the roof of the Department of Physics, lit signs and warning lights on skyscrapers and towers located in the Turin area (at 2 – 4 km distance) were detected, as well as lights from Moncalieri and Chieri towns from the Astrophysical Observatory. In Figure 13 a picture of the “Mole Antonelliana” tower is shown in (a), together with the light curve with time bins of $320 \mu\text{s}$ of one pixel with the signal from the tower (b). The light curve shows an alternating signal with period ~ 35 bins, corresponding to a frequency of ~ 50 Hz, which is consistent with the frequency of the electrical grid. In (c) a picture

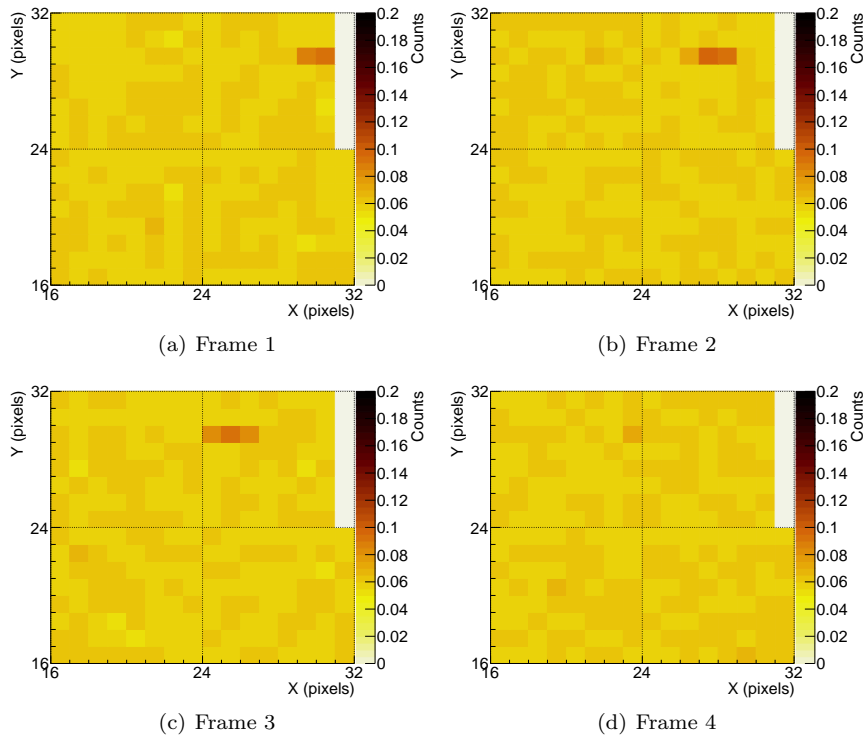


Figure 11: Example of meteor event shown in four consecutive D3 data frames, each integrated over 40.96 ms.

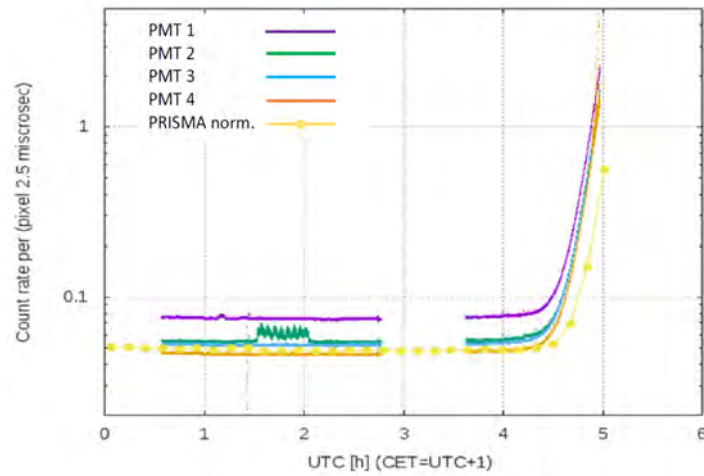
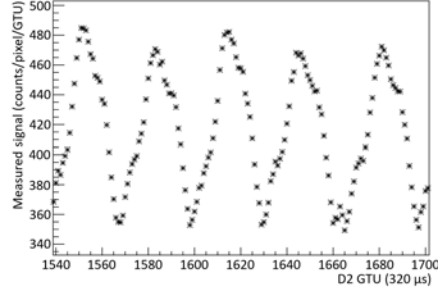


Figure 12: Night sky count rate over time of the four MAPMTs of the Mini-EUSO *EM* and of the PRISMA camera, normalized to the mean value of the three MAPMTs with lower counts.

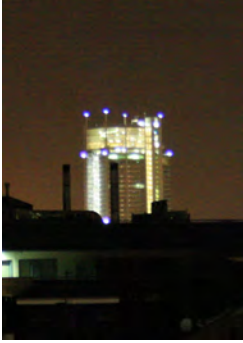
of the “Intesa Sanpaolo” skyscraper with constant emission and white/blue blinking warning lights is shown, together with light curves on two time scales (d). The light curve with time bins of $320 \mu\text{s}$ (left) shows an alternating trend with frequency $\sim 50 \text{ Hz}$, like the tower. The light curve with time bins of 40.96 ms (right) shows high peaks due to flashes that are well above the baseline, pulsating with a frequency of $\sim 0.7 \text{ Hz}$. The $\sim 50 \text{ Hz}$ frequency pattern is present on the baseline and on the



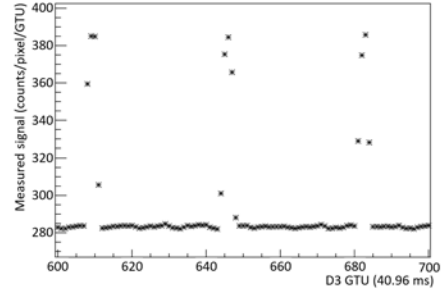
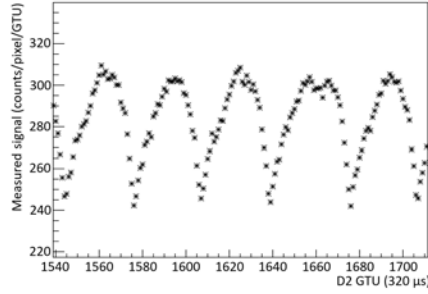
(a) “Mole Antonelliana”



(b) Light curve in D2 timescale



(c) “Intesa Sanpaolo”



(d) Light curve in D2 (left) and D3 (right) timescale

Figure 13: (a) Picture of the “Mole Antonelliana” tower; (b) light curve of one pixel with the signal from the tower, with time bins of $320 \mu\text{s}$ (D2 GTUs), showing the alternating signal with frequency $\sim 50 \text{ Hz}$. (c) Picture of the “Intesa Sanpaolo” skyscraper; (d) light curve of one pixel with the signal from the skyscraper with time bins of $320 \mu\text{s}$, showing the alternating signal with frequency $\sim 50 \text{ Hz}$ (left), and with time bins of 40.96 ms (D3 GTUs), showing flashes from the warning lights with frequency of $\sim 0.7 \text{ Hz}$ (right).

peaks as well. Other buildings with flashers have similar pulsating light curves, and also generic light from cities have light curves with such an alternating profile. This is an important feature of the signal that allows to discriminate between natural and anthropogenic sources. Indeed, with the first observations of the Earth with Mini-EUSO from space it was possible to recognize the modulation of the light current of 50 or 60 Hz depending on the observed area of the globe. It also observed flashes. These observations are described in more details in Section 5.

4.3.2 Rocket of a telecommunication satellite and airplane

During the observations at the Astrophysical Observatory, while pointing to zenith, the orbiting rocket body “Meteor 1-31 Rocket” was detected on 14 March 2018 at 04:10:58 UTC. This device was used for the launch of a telecommunication satellite on 10 July 1981, from the Baikonur Cosmodrome, in Kazakhstan, and was left in orbit as a $2.6 \text{ m} \times 2.8 \text{ m}$ large-size debris orbiting at an average height of $\sim 550 \text{ km}$ and a velocity of $0.8^\circ/\text{s}$ or $\sim 7.5 \text{ km/s}$. The satellite was identified with the Systems Tool Kit (STK) platform [24]. The signal from the satellite is visible in Figure 14 as a bright pixel moving from top-left to bottom-right, in four D3 data frames integrated over 40.96 ms and sampled every $\sim 4 \text{ s}$. The event lasts for 400 D3 GTUs ($\sim 16 \text{ s}$). In the third frame the satellite is not visible as it hits the focal surface in the gap between two MAPMTs. The satellite crosses a length equivalent to ~ 22 pixels in the inclined direction, considering also the

gaps between the MAPMTs. Therefore, the corresponding speed is ~ 1.4 pixel/s.

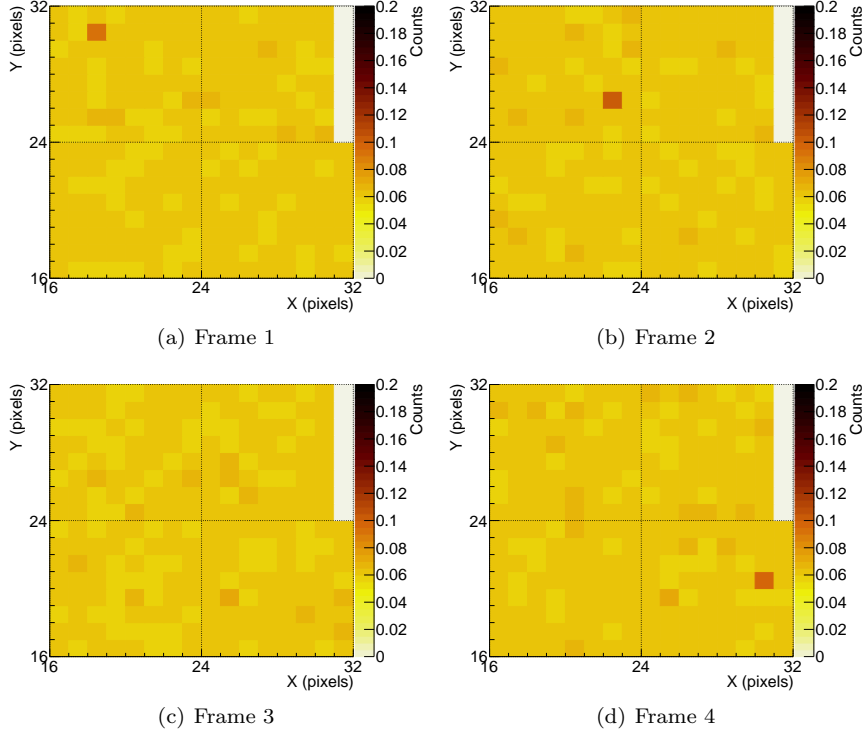


Figure 14: The rocket “Meteor 1-31 Rocket” in four frames integrated over 40.96 ms and sampled every ~ 4 s. The rocket is visible as a bright pixel crossing the field of view from top-left to bottom-right. In one frame the signal is not visible because it hits the focal surface in the gap between two MAPMTs.

This measurement can be translated to an equivalent observation performed by Mini-EUSO. In the case Mini-EUSO would observe an event crossing the field of view with a speed ~ 1.4 pixel/s and considering the field of view of one pixel $0.8^\circ \times 0.8^\circ$, it would correspond to the observation of a space debris with an apparent speed of ~ 0.98 km/s at a distance of 50 km, or a speed of ~ 5.9 km/s at a distance of 300 km from the detector. The apparent speed should be corrected by the ISS speed. More detailed simulation studies and rescaling of the size and distance of this satellite have been done in order to reproduce the detection of space debris with Mini-EUSO on-board the ISS [16].

In addition, flashes of the airplane operating the flight LH1902 from Munich to Turin was detected, from the same site, on 12 March 2018 in the time interval 21:54:2–21:55:12 UTC (about 6 minutes before landing). It passed at an altitude of ~ 780 -690 m above the observation site at 610 m a.s.l., with a speed of 426 km/h. The flight was identified via the Flightradar24 tracking service that provides real-time information about aircrafts around the world [25]. The airplane observation is detailed in Figure 15. Peaks from the four single MAPMTs observing the airplane during its path in the field of view is shown in the top panel, while the signal on the whole EC is visible in the bottom panel. The frequency of the blinking flashes recorded by the EC changes over the time, due to the turning of the airplane while approaching the runway.

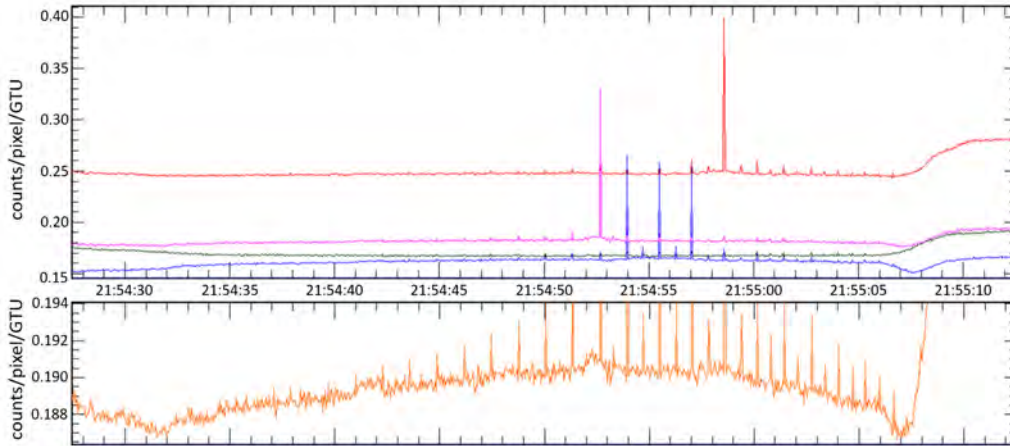


Figure 15: Airplane of the flight LH1902 detected on 12 March 2018 in the time interval 21:54:27–21:55:12 UTC. In the top panel, peaks from four separate MAPMTs are shown. In the bottom panel, peaks from the whole EC are shown: the frequency of the visible flashes changes over the time due to the turning of the airplane while approaching the runway.

5 Comparing Mini-EUSO EM tests with preliminary Mini-EUSO data

As discussed in Section 4.3.1, data acquisitions of artificial light from lit buildings and warning flashers with the Mini-EUSO EM demonstrated the capability of this type of system to detect flashes with frequency ~ 0.7 Hz (seen in D3 data, i.e. with frames integrated over 40.96 ms) and even the modulation of the alternating current, which is 50 Hz in Italy (seen in D2 data, i.e. with frames integrated over 320 μs , see Figure 13). Mini-EUSO from space is also able to detect the modulation of the light current of 50 Hz or 60 Hz depending on the observed area of the globe. Such a modulation is more visible in small towns and villages, that are all connected to the same transformer and therefore emit light in phase. However, it is more difficult to see the modulation in larger cities, where different areas are connected to different transformers, varying phase. Mini-EUSO also observed flashes from several parts of the Earth. Their origin is still under investigation, but they seem to be compatible with warning lights mounted on buildings or towers (usually with xenon, with portion of the emission spectrum in the near-UV). They can have different brightness and duration [5], usually lasting a few hundred μs and being observed several times as they cross the field of view of the detector.

Meteors can also be observed by both detectors. The observation of meteors made with the Mini-EUSO EM was discussed in Section 4.2.2. A definitive confirmation that the observed objects were meteors cannot be obtained because there was no counterpart in the PRISMA camera data, being too faint for PRISMA detectability. However, the estimation of their horizontal speed is consistent with meteors. Moreover, the spatial and temporal development of the meteors observed by Mini-EUSO in orbit, after the necessary rescaling for the distance between detector and source, seem to be compatible with the properties of the objects observed from ground by the Mini-EUSO EM . However, while the apparent magnitude of the meteors observed with the prototype could be estimated thanks to the comparison with the U-band apparent magnitude of field stars, several methods are under study for the estimation of the magnitude of meteors detected from the ISS looking at nadir. Taking as an example the meteor in Figure 11, it is possible to evaluate how Mini-EUSO would have detected the same event from the ISS. Considering that meteors start their development at 100 km from ground, and that the field of view of one pixel of the Mini-EUSO EM is $0.6^\circ \times 0.6^\circ$, the area observed by a pixel at 100 km altitude is ~ 1.0 km \times 1.0 km. A pixel of

Mini-EUSO on the ISS would observe an area of $4.2 \text{ km} \times 4.2 \text{ km}$ at the same altitude (300 km below it), considering the field of view of one pixel as $0.8^\circ \times 0.8^\circ$. As the meteor track appears on 8 pixels, its projection on the horizontal plane at 100 km altitude is $\sim 8.1 \text{ km}$ long. Therefore, Mini-EUSO would have seen the same meteor event in 2 pixels for $\sim 80 \text{ ms}$ ($\sim 40 \text{ ms/pixel}$), while for the Mini-EUSO *EM* it appeared in 8 pixels for $\sim 160 \text{ ms}$ ($\sim 20 \text{ ms/pixel}$).

It is also possible to extrapolate the light source in the case Mini-EUSO observes an event with the same characteristics of the event detected with the Mini-EUSO *EM*, i.e. crossing 8 pixels in $\sim 160 \text{ ms}$. Considering the field of view of $4.2 \text{ km} \times 4.2 \text{ km}$ per pixel at a distance of 300 km from Mini-EUSO, the light source would have a speed of $\sim 210 \text{ km/s}$ (i.e. an angular speed of $\sim 0.7 \text{ rad/s}$ with respect to Mini-EUSO). Such a speed would be compatible with the speed of an interstellar meteor or a nuclearite, although a similar event would not indicate a unique origin. On the other hand, the same speed could correspond to a source traveling with speed $\sim 7.7 \text{ km/s}$ at 389 km altitude, which could be interpreted as a space debris or a satellite lit by the Moon or even the Sun in case of proper sun shield of the detector (as if sunlight reaches the detector, this would be in protection-mode to not damage the device). The calibration of the detector will be fundamental to identify signals of unclear origin.

6 Conclusions

The observations made with the Mini-EUSO *EM* offered the possibility to test the prototype of the Mini-EUSO detector that was launched and installed on the ISS in 2019. The tests described in this paper provided a large variety of data on different timescales, by which the detector performance was studied.

Tests at TurLab demonstrated that some improvements for L1 trigger had to be performed, while the L2 trigger algorithm and the continuous data acquisition proved to work as expected. With a new system, which is basically a copy of the Mini-EUSO *EM* detector regarding the data acquisition and the processing, further studies were performed afterwards. A new threshold of 16σ has been applied to the L1 trigger, that made it more robust and stronger against the non-standard background condition (much lower or higher than $\sim 1 \text{ count/pixel/GTU}$) and was applied to the firmware of Mini-EUSO. Moreover, tests to estimate the reflectance of materials that compose space debris were performed, together with simulation analyses to study the capability of JEM-EUSO-like instruments to detect and track space debris from space.

Outdoor data acquisitions allowed to detect several natural and artificial light sources. Stars with apparent magnitude up to ~ 4 permitted a comparison between the performance of the Mini-EUSO *EM* and the PRISMA camera of the Astrophysical Observatory of Turin. The possible detection of meteors showed that the telescope is able to detect faint meteors with speeds of the order of tens of kilometers per second. The analysis of the night sky brightness detected at the zenith before sunrise showed that the signal in the UV band increased earlier than in the visual band, consistent with the fact that the UV photons are more scattered than the visual ones. Observations of artificial light from buildings showed the capability of detecting flashes from warning lights with frequencies of 0.7 Hz and the modulation of the current of 50 Hz. Finally, with the detection of a known space debris, it was possible to rescale the size and the distance to emulate the detection of space debris by Mini-EUSO from space.

Observations of similar sources have been made by both the Mini-EUSO *EM* during the outdoor tests and Mini-EUSO from the ISS. This is the case for flashes, the modulation of the alternating signal from the electrical grid, and meteors. The experience acquired before the Mini-EUSO launch with the engineering model allowed to predict some of the observations that can be made from space and to understand how to interpret them, for example using the modulation of the current to distinguish between artificial and natural light (such as bioluminescence).

The results and studies discussed in this paper revealed important for the analysis and operation of the Mini-EUSO telescope. Mini-EUSO already confirmed some expectations raised during the tests of the engineering model.

Acknowledgments

The authors acknowledge all members of the JEM-EUSO Collaboration, especially the Mini-EUSO team. Special thanks also to Andreas Haungs and Jacek Szabelski for their detailed and very useful internal review of the paper. This work was supported by State Space Corporation ROSCOSMOS, by the Italian Space Agency through the ASI INFN agreement n. 2017-8-H.0 and contract n. 2016-1-U.0, by Basic Science Interdisciplinary Research Projects of RIKEN and JSPS KAKENHI Grant (JP17H02905, JP16H02426 and JP16H16737), by the Italian Ministry of Foreign Affairs and International Cooperation, by the French space agency CNES. PRISMA was funded by 2016/0476 and 2019/0672 Research and Education grants from Fondazione Cassa di Risparmio di Torino and by a 2016 grant from Fondazione Agostino De Mari (Savona). The authors from the University of Turin acknowledge support from Compagnia di San Paolo within the project “ex-post-2018”.

References

- [1] S. Bacholle et al., “Mini-EUSO mission to study Earth UV emissions on board the ISS”, accepted for publication in *Astrophysical Journal Supplement Series* (2020); preprint available at arXiv:2010.01937v1
- [2] J.H. Adams Jr. et al. (JEM-EUSO Coll.), “JEM-EUSO observational technique and exposure”, *Exp. Astron.*, v.40, pp.117-134 (2015)
- [3] J.H. Adams Jr. et al., “JEM-EUSO: Meteor and nuclearite observations”, *Exp. Astron.* v.40, pp.253-279 (2015)
- [4] T. Ebisuzaki et al., “Demonstration designs for the remediation of space debris from the International Space Station”, *Acta Astronautica* 112 (2015)
- [5] J.H. Adams et al., “Calibration for extensive air showers observed during the JEM-EUSO mission”, *Advances in Space Research*, v.53, pp.1506-1514 (2014)
- [6] G. Abdellaoui et al., “First observations of speed of light tracks by a fluorescence detector looking down on the atmosphere”, *Journal of Instrumentation*, vol. 13, P05023 (2018)
- [7] V. Kungel et al. (JEM-EUSO Coll.), “Laser test with Mini-EUSO”, *PoS(ICRC2019)325* (2019)
- [8] TurLab URL: <http://www.turlab.ph.unito.it/>
- [9] H. Prieto-Alfonso et al. (JEM-EUSO Coll.), “Multi anode photomultiplier tube reliability assessment for the JEM-EUSO space mission”, *Proc. of ICRC2013* (2013)
- [10] S. Blin-Bondil et al., “SPACIROC3: A Front-End Readout ASIC for JEM-EUSO cosmic ray observatory”. *Proc. of TIPP 2014*, *PoS(TIPP2014)172* (2014).
- [11] F. Capel et al., “Mini-EUSO (Extreme Universe Space Observatory) data acquisition and control software”. *The Journal of Astronomical Telescopes, Instrumentation and Systems*, v.5(4), pp.044009 (2019)
- [12] A. Belov et al., “The integration and testing of the Mini-EUSO multi-level trigger system”, *Advances in Space Research*, v.62, pp.2966-2976 (2018)
- [13] H. Miyamoto et al. (JEM-EUSO Coll.), “The EUSO@TurLab Project” *Proc. of the XXV European Cosmic Ray Symposium* (2016)
- [14] G. Suino et al. (JEM-EUSO Coll.), “The EUSO@Turlab Project: Results from Phase II”, *PoS(ICRC2017)422* (2017)

- [15] Xilinx. Zynq-7000 All Programmable SoC (2016)
URL: <https://www.xilinx.com/products/silicon-devices/soc/zynq-7000.html>
- [16] H. Miyamoto et al. (JEM-EUSO Coll.), “Space debris detection and tracking with the techniques of cosmic ray physics”, PoS(ICRC2019)253 (2019)
- [17] F. Fenu et al. (JEM-EUSO Coll.), “Simulations for the JEM-EUSO program with ESAF” PoS(ICRC2019)252 (2019)
- [18] MASTER ESA’s software to assess the debris or meteoroid flux imparted on a spacecraft on an arbitrary Earth’s orbit. URL: <https://sdup.esoc.esa.int/>
- [19] D. Gardiol et al., “News from the Italian PRISMA fireball network”, Proc. of the 37th International Meteor Conference, pp.81-86 (2019)
- [20] D. Gardiol et al., “Cavezzo, the first Italian meteorite recovered by the PRISMA fireball network. Orbit, trajectory, and strewn-field”, submitted to Monthly Notices of the Royal Astronomical Society (2020)
- [21] D. Barghini et al., “Improving astrometry and photometry reduction for PRISMA all-sky cameras”, Proc. of the 37th International Meteor Conference, pp.41-45 (2020)
- [22] D. Barghini et al., “Astrometric calibration for all-sky cameras revisited”, Astronomy & Astrophysics, 626, A105 (2019)
- [23] G. Abdellaoui et al., “Meteor studies in the framework of the JEM-EUSO program”, Planetary and Space Science, v143, pp.245-255 (2017)
- [24] URL: <https://www.agi.com/products/stk>
- [25] URL: <https://www.flightradar24.com/>